Electronic Supplementary Material (ESI) for ChemComm.

Stabilisation of an amorphous form of ROY through a predicted co-former interaction

Philip Corner, Jonathan Harburn, Jonathan Steed, James McCabe and David Berry

Supporting Information

1. Synthesis of ROY

Step 1 - 11.68 g (0.364 mol) sulfur, 25.33 g (31.5 ml, 0.436 mol) propionaldehyde and 75 ml DMF were placed in a flange-necked flask fitted with an overhead stirrer, air condenser, thermometer, and dropping funnel. Triethylamine (30.9 ml, 0.222 mol) was added dropwise over 35 minutes to the cooled stirred reaction mixture whilst maintaining the pot temperature between -5-10 °C with an ice-bath. After addition the pot was allowed to warm up to 20 °C over 45 minutes, keeping the mixture well stirred. A solution of 24.1 g (0.365 mol) malononitrile in 50 ml DMF was added drop-wise over 60 minutes keeping the pot temperature between 8-20 °C throughout the addition. Once complete the mixture was stirred at 15-20 °C for a further 45 minutes then sampled for TLC. The mixture was then poured onto approx. 600 ml ice/water with stirring to cause the required product to precipitate for around 1 hour. After 10 minutes the stirrer was switched off and the solid allowed to settle. The aqueous liquor was decanted away and the solid isolated by filtration. The solid was left to dry for approximately 65 hours. The isolated solid was well washed with 215 ml deionised water, then dried overnight in vacuo at 70-75 °C to give 2-amino-5-methylthiophene-3-carbonitrile.

Step 2 - A solution of 32.05 g (0.227 mol) 2-fluoronitrobenzene and 31.36 g (0.227 mol) 2-amino-5-methylthiophene-3-carbonitrile in 285 ml dry THF was added dropwise to a stirred slurry of 16.36 g (0.682 mol) sodium hydride in 57 ml dry THF under nitrogen. The mixture was stirred at 25 °C for 24 hours, poured onto cracked ice and extracted into DCM (3 x 570 ml). The combined extracts were washed with 2N HCL (2 x 225 ml) and water (2 x 225 ml), dried over magnesium sulfate and the solvent removed under reduced pressure. The residue was crystallised from ethanol to give ROY.

2. Analysis of synthesised ROY

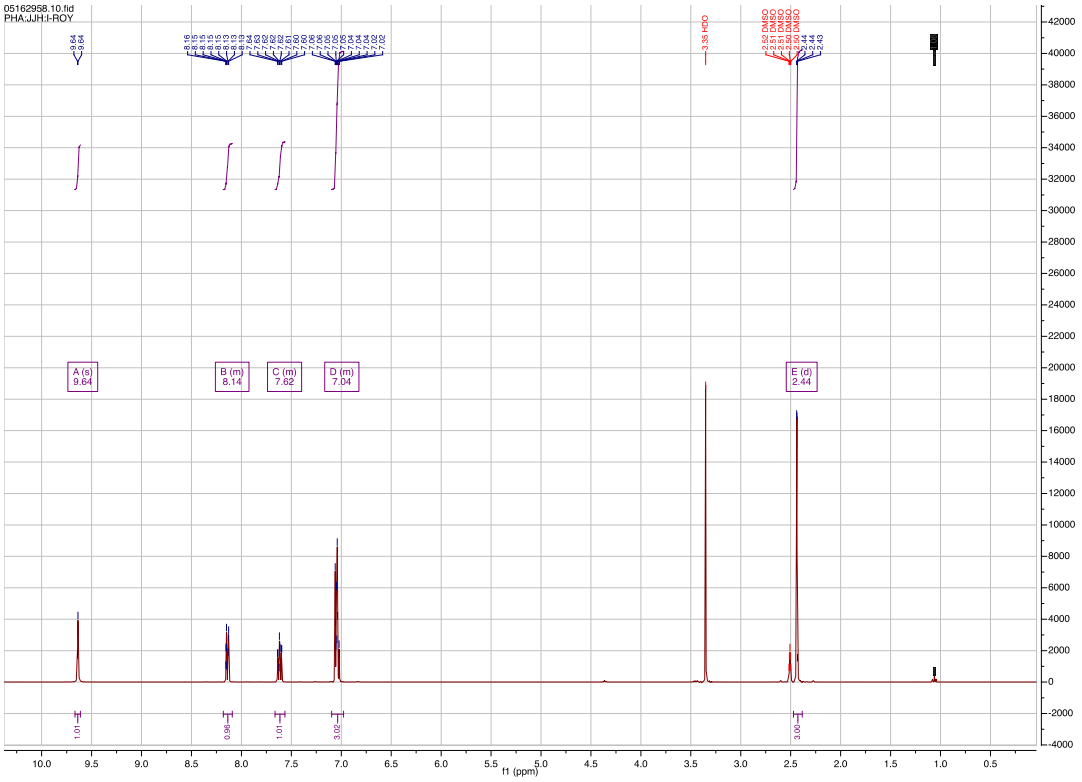

Figure S1. ^{1}H NMR spectrum of synthesised ROY

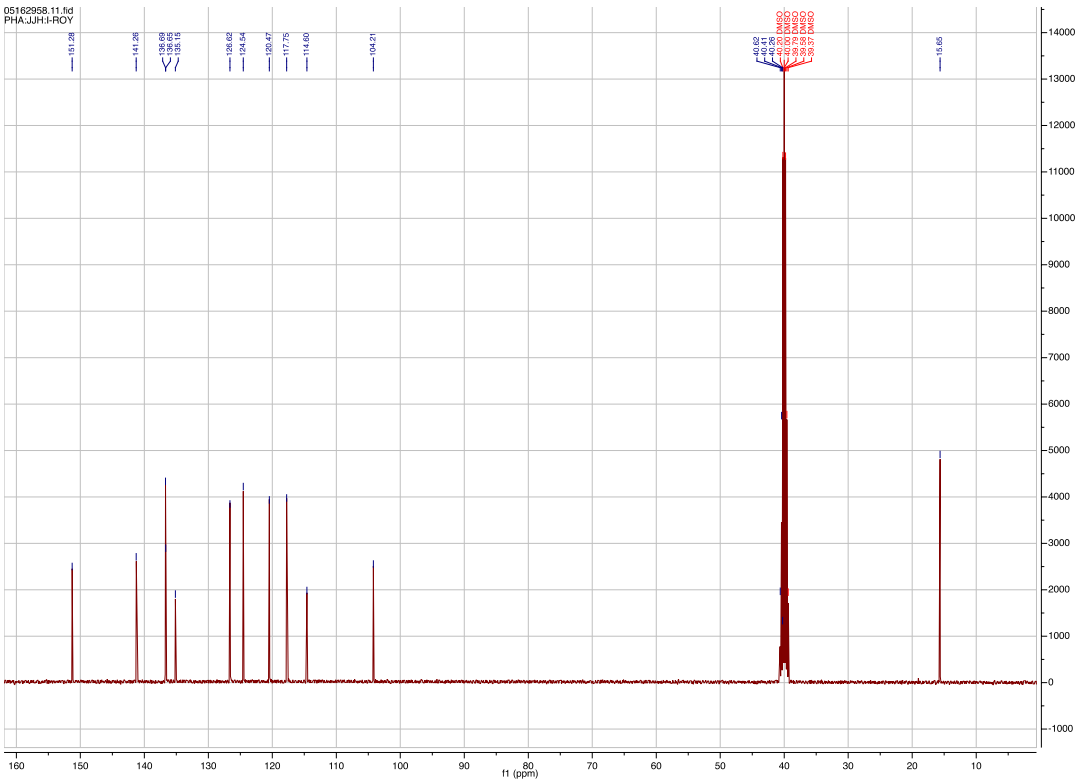

Figure S2. ^{13}C NMR spectrum of synthesised ROY

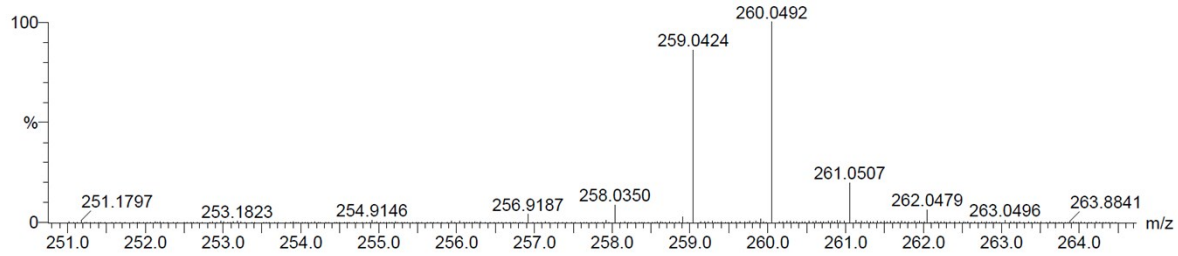

Minimum:				-1.5			
Maximum:		3.0	5.0	50.0			
Mass	Calc. Mass	mDa	PPM	DBE	i-FIT	i-FIT (Norm)	Formula
260.0492	260.0494	-0.2	-0.8	9.5	354.0	0.0	C12 H10 N3 O2 S

Figure S3. Accurate mass mass spectrum of synthesised ROY

ROY = $C_{12}H_9N_3O_2S$ = 259.041549

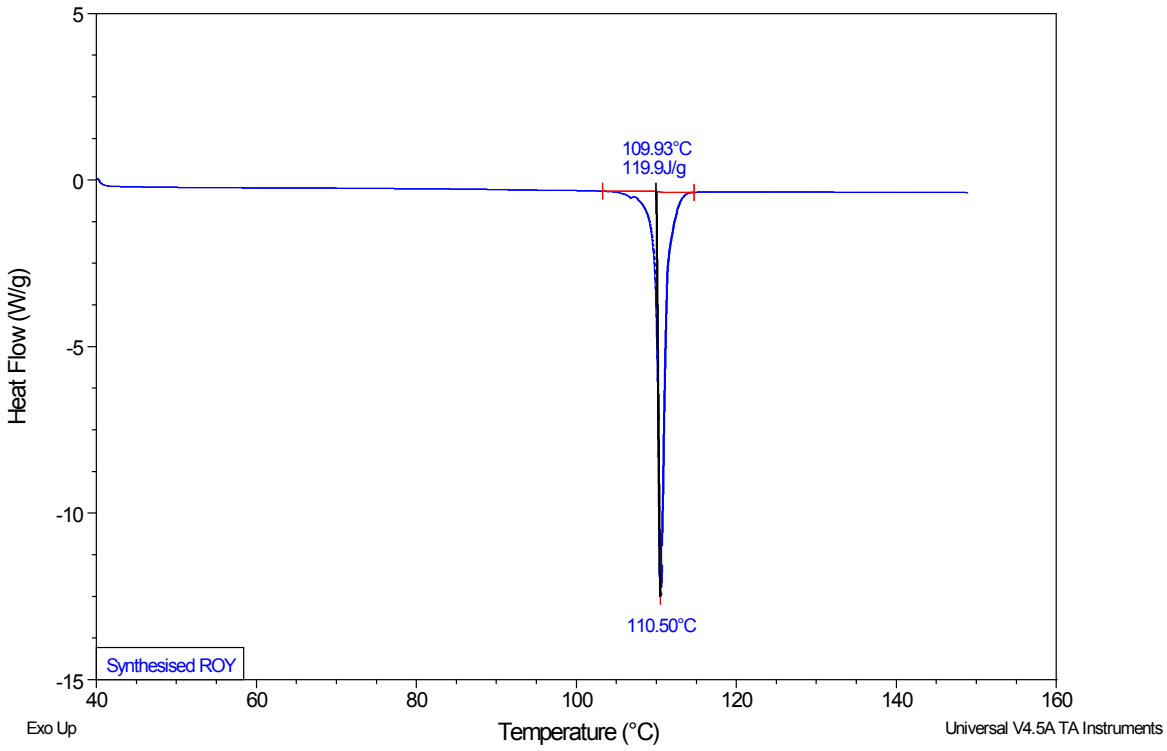

Figure S4. DSC trace for synthesised ROY

Melting point (onset) = 109.93°C. This is commensurate with polymorph Y.[1]

3. Materials and experimental details

Materials. ROY was synthesised following the procedure reported in the patent for the synthesis of Olanzapine. Analysis of the produced substance can be found in section 2. Pyrogallol and Polyvinylpyrrolidone (average molecular weight 40,000) were purchased from Sigma-Aldrich (UK), were of at least reagent grade and used as received. Acetone was obtained from Sigma-Aldrich, was of HPLC grade and used as received.

Computational (*in silico*) prediction. COSMOtherm software was used to perform the calculations for prediction of compounds likely to act as co-formers, forming co-crystals with a particular API. This modelling led to a list of energetically favourable combinations of co-former to ROY (Seen in ESI Table S10 (full) and Table S11 (condensed with FTIR data)) and those with the greatest enthalpic driver for interaction were taken forwards to the physical screen.

Production of the amorphous cell was completed in Materials Studio (Dassault Systemes, BIOVIA Ltd.) with molecular conformations taken from the entries in the Cambridge Structural Data base. A cell of 100 of each molecule (1:1 ratio ROY and pyrogallol) was then produced with charges defined by Gasteiger, utilising a Dreiding forcefield. This was then allowed to minimise.

Physical co-crystal screen. A method of co-crystal production employing ultrasonication was developed in which 25mg of ROY dissolved in a DCM solution was added to an equimolar amount of solid, previously weighed, potential co-former in 48 wells of a borosilicate glass 96-well plate (picture of set-up shown in Figure S5). After leaving the initial solvent to evaporate, 50 µl of acetone was added to 8 wells and the 8-tips of the ultrasonic probe were placed in these wells and sonicated at 50% power for 10 minutes using a Sonics Vibra Cell 130 W 20 kHz ultrasonic processor. This process was repeated for the remaining wells and the whole process repeated a further two times replacing acetone as the solvent with ethanol and hexane respectively; thereby completing the screening process in three solvents for 48 potential co-formers. The optimal parameters for each solvent varied slightly, for example a higher temperature was used with Hexane.

X-ray Powder Diffraction (XRPD). X-ray powder diffraction patterns were recorded on a PANalytical Empyrean diffractometer using Cu Kα radiation (λ = 1.54 Å), tube voltage of 40 kV and 40 mA current. Intensities were measured from 2° to 40° 2θ with 0.04 rad. Soller silts and an incident beam divergent slit of 1/8°, anti-scatter slit of 1/4° and diffracted beam anti-scatter slit of 7.5mm (PIXcel).

Differential Scanning Calorimetry (DSC). Differential scanning calorimetry scans were recorded on a TA Q2000 using standard aluminium pans. Standard mode was used throughout and where heat/cool/heat cycles was used the initial heating phase was at a rate of 10°C/min, cooling cycle at 50°C/min and the second heating cycle at 10°C/min.

Infrared (IR) Spectroscopy. FTIR spectra of solid phases were collected on either an Agilent Cary 630 FTIR spectrometer with diamond attenuated total reflectance (ATR) crystal accessory and 128 scans for each sample were collected at a resolution of 2 cm^{-1} over a wavenumber region of 4000-650 cm^{-1}; or a PerkinElmer Spectrum Two FTIR spectrometer with diamond universal ATR accessory and 4 scans for each sample were collected at a resolution of 2 cm^{-1} over a wavenumber region of 4000-600 cm^{-1}.

Liquid-Assisted Grinding (LAG). Approximately 50 mg of ROY was weighed out, and with an equimolar equivalent of potential co-former, placed in a mortar. An addition of 25 µl of acetone occurred before grinding by hand with a pestle for 5 minutes. This process was repeated for each of the top 10 predicted potential co-formers for ROY. The products were analyses by FTIR.

Evaporative Crystallisation. Saturated solutions in acetonitrile of each of the top 10 predicted potential co-formers for ROY were produced and 1ml of each placed in 10 vials. To each of these 1 ml of a saturated solution of ROY in acetonitrile was added. The vials were shaken and left to allow evaporation of the solvent. The products were analysed by XRPD.

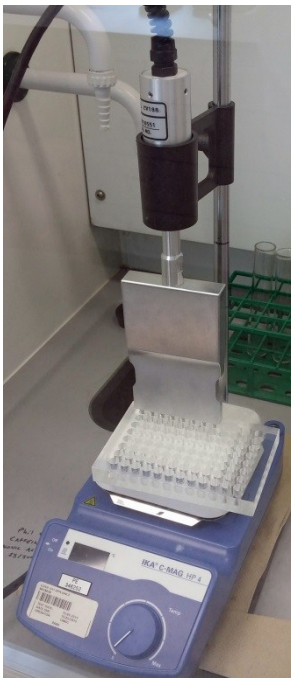

Figure S5. Photograph showing experimental setup including (from top): ultrasonic probe (Sonics Vibra Cell, 130W, 20kHz), 8-tip probe adapter, 96-well plate (Zinsser, borosilicate glass), hot plate.

4. FTIR data for the analysis of the physical co-crystal screen and further investigations

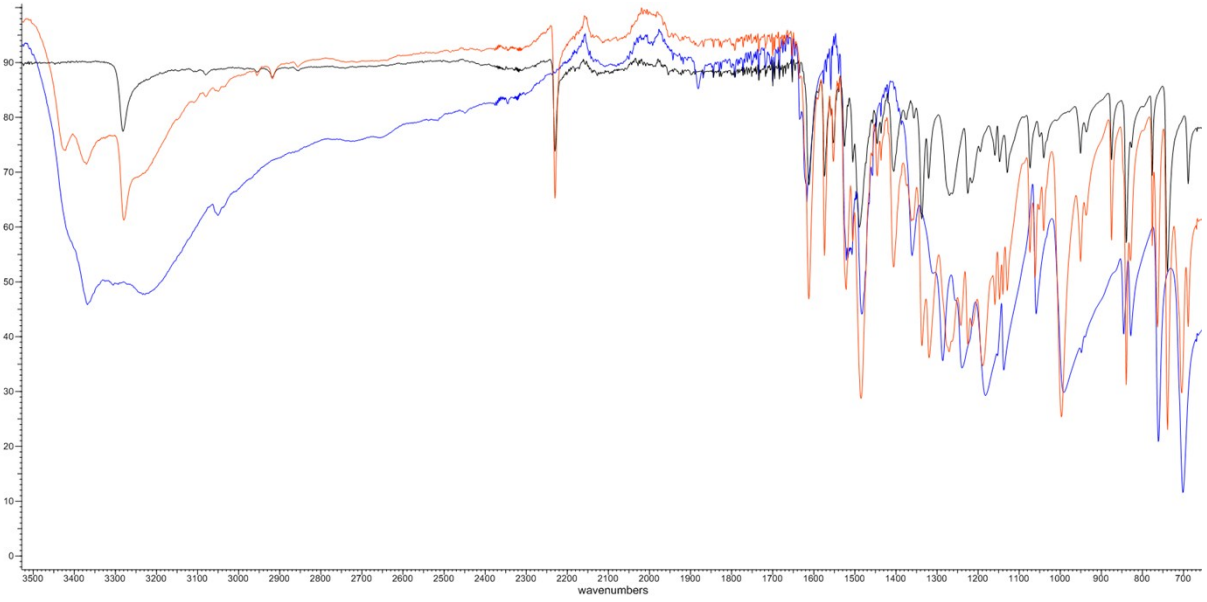

Figure S6. FTIR spectra of ROY (black), pyrogallol (blue) and the 1:1 grind of these components (orange).

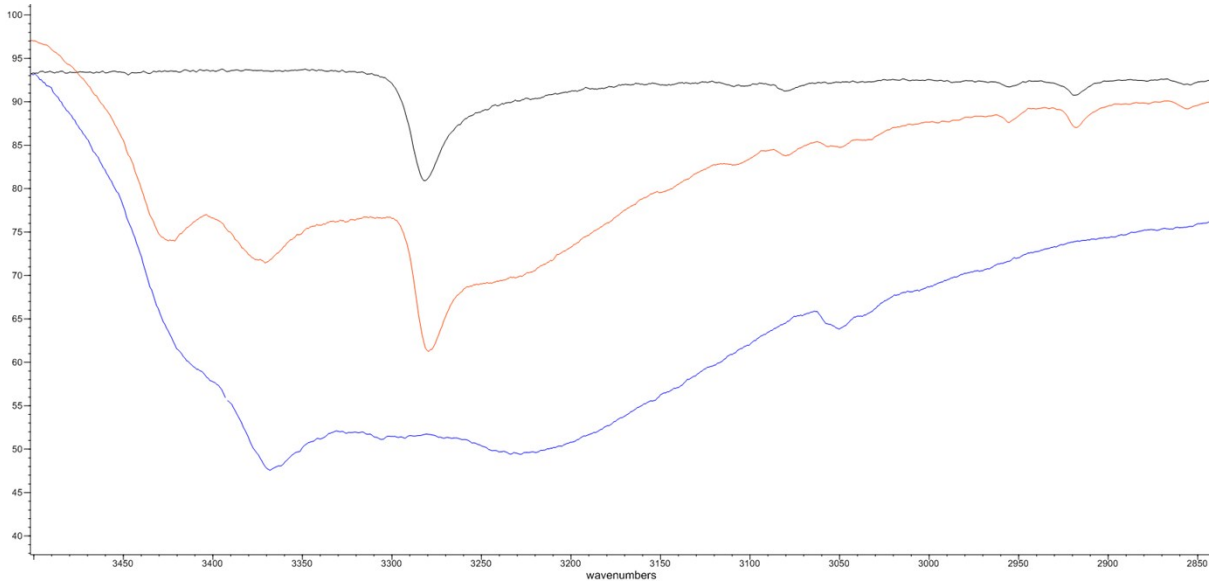

Figure S7. Subset of FTIR spectra in Figure S6 showing peaks at higher wavenumbers in greater detail; ROY (black), pyrogallol (blue) and the 1:1 grind of these components (orange).

Figures S6 and S7 show that absorption peaks observed in the ROY:Pyrogallol 1:1 grind occur at the same wavenumber as the corresponding peaks in the spectra of the pure/parent materials and as such are indicative that bonding within the material is not significantly altered, as would be likely if hydrogen bonds between the ROY and pyrogallol were to be form.

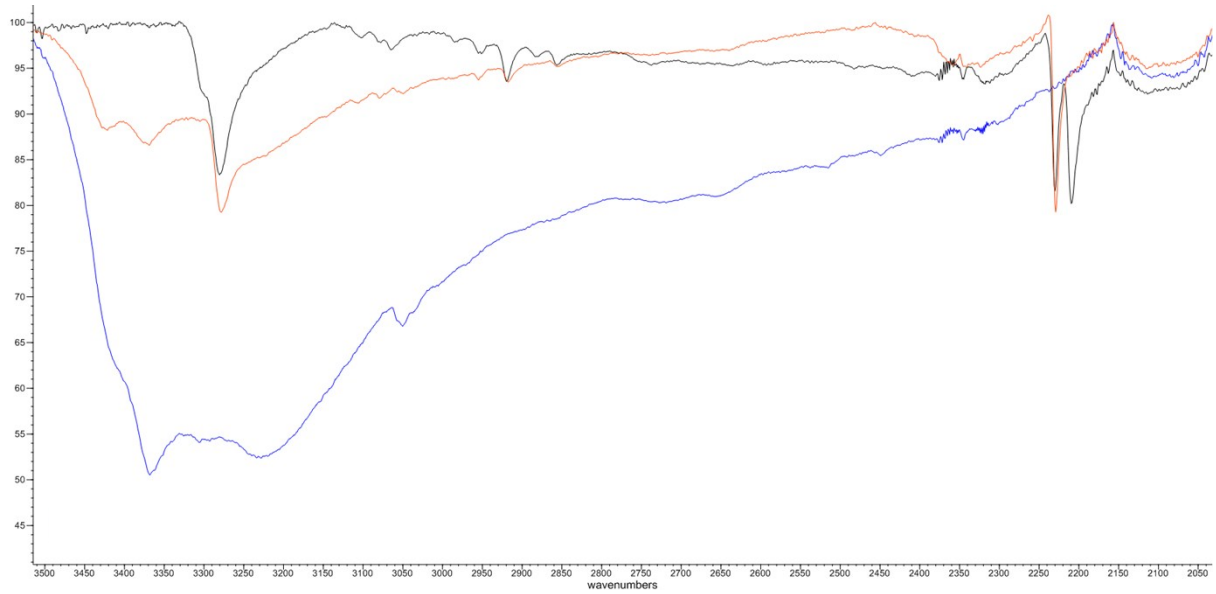

Figure S8. FTIR spectra of ROY (black), pyrogallol (blue) and the product from the co-crystal screening of these two components (orange),showing only the wavenumber region from 2000 to 3500 cm-1.

The same outcome as above in seen in Figure S8, in that the screen did not indicate co-crystal formation. The presence of an extra peak in the spectrum of ROY at around 2200 is due to the presence of a second polymorph within the sample analysed.

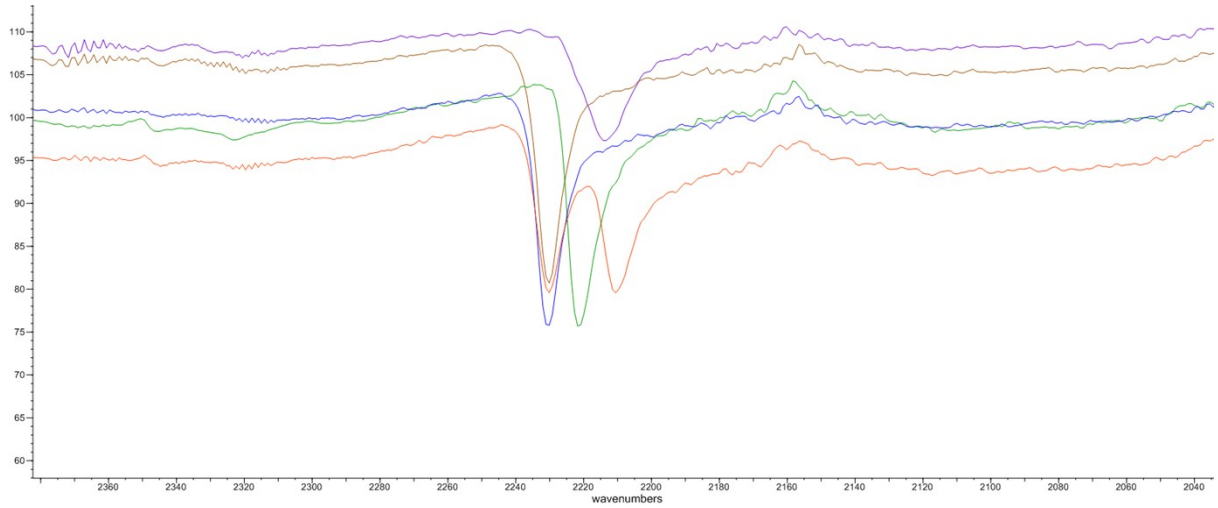

Figure S9. FTIR spectra of a number of ROY polymorphs and a combination thereof.

The spectra displayed in Figure S9 are of polymorphs of ROY (obtained by evaporation from different solvents) and provide the reference wavenumbers for which Table S11 below compares the products of screening to determine indication of significant intermolecular interaction.

5. Ranked list of co-formers based on COSMOtherm calculations

Table S10. List of co-formers with excess enthalpy calculated for the given stoichiometry with ROY as produced by COSMOtherm

Co-Former Name	DH / kJ.mol^{-1}	Stoichiometry
Pentafluorophenol_c0	-1.95304667	"1:2"
Pentafluorophenol_c0	-1.83812	"1:1"
Acesulfame	-1.508955	"1:1"
Acesulfame	-1.38306667	"1:2"
Pentafluorophenol_c0	-1.37965333	"2:1"
OXALIC_ACID	-1.345755	"1:1"
Quercetin	-1.296365	"1:1"
Quercetin	-1.29356	"2:1"
Acesulfame	-1.26151667	"2:1"
OXALIC_ACID	-1.22758	"2:1"
SULFAMIC_ACID	-1.22224	"1:1"
3_5_Dinitrobenzoic_Acid	-1.19337	"1:1"
OXALIC_ACID	-1.1712	"1:2"
1,2,3-Trihydroxybenzene	-1.144635	"1:1"
SULFAMIC_ACID	-1.12732333	"2:1"
SULFAMIC_ACID	-1.08531667	"1:2"
3_5_Dinitrobenzoic_Acid	-1.06875333	"1:2"
2,4-dihydroxybenzoic_acid	-1.04422	"1:1"
3_5_Dinitrobenzoic_Acid	-1.04109333	"2:1"
5-nitroisophthalic_acid	-1.036695	"1:1"
Quercetin	-1.03450333	"1:2"
Gallic_acid	-1.031715	"1:1"
1,2,3-Trihydroxybenzene	-1.03138333	"2:1"
TERT-BUTYLHYDROQUINONE	-1.02651	"1:1"
5-nitroisophthalic_acid	-0.99448	"2:1"
1-hydroxy-2-naphthoic_acid	-0.99384	"1:1"
Catechol	-0.98762	"1:1"
1,2,3-Trihydroxybenzene	-0.98737	"1:2"
4-Hexylresorcinol	-0.98664	"1:1"
1-hydroxy-2-naphthoic_acid	-0.95433	"1:2"
2,4-dihydroxybenzoic_acid	-0.95418667	"2:1"
TERT-BUTYLHYDROQUINONE	-0.94342	"1:2"
Gallic_acid	-0.942	"2:1"
Catechol	-0.92858667	"1:2"
2,4-dihydroxybenzoic_acid	-0.90741	"1:2"
4-Hexylresorcinol	-0.90391667	"1:2"
5-chlorosalicylic_acid	-0.902455	"1:1"
Gallic_acid	-0.90101667	"1:2"
RESORCINOL	-0.897925	"1:1"
P-VINYLPHENOL_c0	-0.89657	"1:1"

P-VINYLPHENOL_c0	-0.89029333	"1:2"
TERT-BUTYLHYDROQUINONE	-0.87088	"2:1"
3,5-dihydroxybenzoic_acid	-0.86552	"1:1"
5-nitroisophthalic_acid	-0.86511	"1:2"
4-Hexylresorcinol	-0.84925667	"2:1"
RESORCINOL	-0.83844	"1:2"
5-chlorosalicylic_acid	-0.8336	"1:2"
Catechol	-0.82803667	"2:1"
3,5-dihydroxybenzoic_acid	-0.81828667	"2:1"
1-hydroxy-2-naphthoic_acid	-0.81693333	"2:1"
RESORCINOL	-0.77271	"2:1"
5-chlorosalicylic_acid	-0.76804333	"2:1"
Orcinol	-0.768	"1:1"
2,5-dihydroxybenzoic_acid	-0.762985	"1:1"
gentisic_acid	-0.756395	"1:1"
3,5-dihydroxybenzoic_acid	-0.74557667	"1:2"
P-VINYLPHENOL_c0	-0.71876667	"2:1"
Orcinol	-0.71534333	"1:2"
2,5-dihydroxybenzoic_acid	-0.69776667	"2:1"
gentisic_acid	-0.69399333	"2:1"
O-CRESOL	-0.68783	"1:1"
O-CRESOL	-0.67925	"1:2"
3_4-DIHYDROXYBENZOIC_acid	-0.675945	"1:1"
2,5-dihydroxybenzoic_acid	-0.67136333	"1:2"
THYMOL	-0.66492	"1:1"
gentisic_acid	-0.66227333	"1:2"
Orcinol	-0.66176333	"2:1"
THYMOL	-0.66030667	"1:2"
PHENOL_c0	-0.65244	"1:2"
trimesic_acid	-0.64779667	"2:1"
PHENOL_c0	-0.645445	"1:1"
trimesic_acid	-0.625265	"1:1"
3_4-DIHYDROXYBENZOIC_acid	-0.61500667	"2:1"
INDOLE_c0	-0.598635	"1:1"
INDOLE_c0	-0.59816	"1:2"
3_4-DIHYDROXYBENZOIC_acid	-0.59177333	"1:2"
3-hydroxy-2-naphthoic_acid	-0.58607	"1:1"
2,5-Xylenol	-0.582905	"1:1"
2_5-XYLENOL	-0.58251	"1:1"
2,5-Xylenol	-0.57731	"1:2"
2_5-XYLENOL	-0.57632333	"1:2"
salicylic_acid	-0.569225	"1:1"
m-nitrobenzoic_acid	-0.566095	"1:1"
SKATOLE_c0	-0.55596	"1:2"

O-CRESOL	-0.55326	"2:1"
SKATOLE_c0	-0.552105	"1:1"
Hydroquinone_c0	-0.552085	"1:1"
FUMARIC_ACID	-0.549575	"1:1"
3-hydroxy-2-naphthoic_acid	-0.53992	"1:2"
Hydroquinone_c0	-0.53467333	"1:2"
FUMARIC_ACID	-0.53440667	"2:1"
THYMOL	-0.52590333	"2:1"
methylgallate	-0.524405	"1:1"
salicylic_acid	-0.5235	"1:2"
PHENOL_c0	-0.51339333	"2:1"
m-nitrobenzoic_acid	-0.50407667	"2:1"
3-hydroxy-2-naphthoic_acid	-0.50406	"2:1"
m-nitrobenzoic_acid	-0.50092	"1:2"
trimesic_acid	-0.49986667	"1:2"
P-CRESOL	-0.49931333	"1:2"
salicylic_acid	-0.48972	"2:1"
P-CRESOL	-0.4879	"1:1"
Methanesulfonic	-0.482445	"1:1"
Methanesulfonic	-0.47865333	"2:1"
INDOLE_c0	-0.47527333	"2:1"
methylgallate	-0.47443667	"1:2"
P-ETHYLPHENOL_c0	-0.47219333	"1:2"
3-HYDROXYBENZOIC_ACID	-0.469155	"1:1"
2_5-XYLENOL	-0.46777333	"2:1"
2,5-Xylenol	-0.46765333	"2:1"
FUMARIC_ACID	-0.46547667	"1:2"
methylgallate	-0.46515667	"2:1"
Hydroquinone_c0	-0.46011333	"2:1"
P-ETHYLPHENOL_c0	-0.459365	"1:1"
6-hydroxy-2-naphthoic_acid	-0.449685	"1:1"
Ethanesulfonic_acid	-0.448055	"1:1"
SKATOLE_c0	-0.43566	"2:1"
Ethanesulfonic_acid	-0.43312667	"2:1"
3-HYDROXYBENZOIC_ACID	-0.43194	"2:1"
ALLOCITRIC_ACID	-0.42774	"1:1"
p-tButyl-PHENOL_c0	-0.42679333	"1:2"
3,4-Xylenol_c0	-0.41840667	"1:2"
ISOCITRIC_ACID	-0.41742	"1:1"
3_4-xylenol_c0	-0.41659667	"1:2"
3-HYDROXYBENZOIC_ACID	-0.4129	"1:2"
p-tButyl-PHENOL_c0	-0.40929	"1:1"
6-hydroxy-2-naphthoic_acid	-0.40685333	"2:1"
ALLOCITRIC_ACID	-0.40594333	"1:2"

3,4-Xylenol_c0	-0.40526	"1:1"
3_4-xylenol_c0	-0.40316	"1:1"
6-hydroxy-2-naphthoic_acid	-0.39945667	"1:2"
2_6-xylenol_c0	-0.39238333	"1:2"
P-CRESOL	-0.38472667	"2:1"
ISOCITRIC_ACID	-0.38090667	"2:1"
2_6-xylenol_c0	-0.3799	"1:1"
ISOCITRIC_ACID	-0.37862	"1:2"
Methanesulfonic	-0.37413667	"1:2"
citric_acid	-0.373535	"1:1"
Etidronic_acid	-0.36914333	"1:2"
4-HYDROXYBENZOIC_ACID	-0.367105	"1:1"
ALLOCITRIC_ACID	-0.36153	"2:1"
P-ETHYLPHENOL_c0	-0.36051333	"2:1"
O-PHENYLPHENOL	-0.35926	"1:1"
Ethanesulfonic_acid	-0.3506	"1:2"
Etidronic_acid	-0.350515	"1:1"
citric_acid	-0.34377333	"1:2"
O-PHENYLPHENOL	-0.33863	"1:2"
citric_acid	-0.33800667	"2:1"
4-HYDROXYBENZOIC_ACID	-0.33745667	"1:2"
4-HYDROXYBENZOIC_ACID	-0.32179333	"2:1"
2-OXO-3-PHENYLPROPIONIC_ACID	-0.32097	"1:1"
3,4-Xylenol_c0	-0.31694667	"2:1"
p-tButyl-PHENOL_c0	-0.31617667	"2:1"
3_4-xylenol_c0	-0.31507667	"2:1"
O-PHENYLPHENOL	-0.30168333	"2:1"
2_6-xylenol_c0	-0.29408	"2:1"
2-OXO-3-PHENYLPROPIONIC_ACID	-0.28822667	"1:2"
2-OXO-3-PHENYLPROPIONIC_ACID	-0.28083667	"2:1"

6. Results from FTIR analysis of physical co-crystal screen

Table S11. COSMOtherm rank order of co-formers used for ROY Screen (48 selected from the top 49 predicted using COSMOtherm with 1 excluded due to availability (p-Vinylphenol #17)) and the screening outcome.

Number	Co-former	~3300 peak (acetone)	~2220 peak (acetone)	~3300 peak (ethanol)	~2220 peak (ethanol)	~3300 peak (hexane)	~2220 peak (hexane)
1	Pentafluorophenol	3280	2209+2230	3280	2229	3003+3281	2210+2230
2	Acesulfame	3280	2209+2230	3280	2210+2230	3280	2210+2230
3	Oxalic acid	3282+3302	2209+2230	3279	2228	3281	2221+2230
4	Quercetin	3280	2230	3279	2230	3280	2222+2230
5	Sulfamic acid	3280	2229	3280	2229	3283	2221
6	3,5-Dinitrobenzoic acid	3280	2210+2229	3280	2230	3281	2223+2229
7	1,2,3-Trihydroxybenzene	3278	2229	3279	2229	3280	2230
8	2,4-Dihydroxybenzoic acid	3280	2229	3280	2230	3282	2222+2230
9	5-Nitroisophthalic acid	3278	2229	3278	2229	3281+3300	2210+2230
10	Gallic acid	3277	2209+2229	3276	2228	3278	2209+2230
11	tert-Butylhydroquinone	3280	2230	3279	2229	3281	2211+2230
12	1-Hydroxy-2-naphthoic acid	3279	2230	3282+3300	2209+2230	3280	2216+2230
13	Catechol	3278	2229	3279	2230	3282	2218+2230
14	4-Hexylresorcinol	3280	2229	3281	2226	3334	2223
15	5-Chlorosalicylic acid	3278	2229	3278	2229	3281	2222
16	Resorcinol	3277	2209+2229	3279	2230	3306	2227
17	3,5-Dihydroxybenzoic acid	3278	2209+2229	3279	2230	3281	2210+2230
18	Orcinol	3279	2229	3279	2229	3292	2221
19	2,5-Dihydroxybenzoic acid	3278	2229	3280	2210+2230	3280	2230
20	o-Cresol	3280	2229	3278	2229	3283	2222
21	3,4-Dihydroxybenzoic acid	3280	2230	3278	2229	3281	2229
22	Thymol	3279	2229	3279	2229	3282	2222
23	Phenol	3280	2229	3281	2230	3280	2221+2230
24	Trimesic acid	3280	2210+2230	3280	2229	3280	2222+2230
25	Indole	3279	2229	3300	2218	3297	2217
26	3-Hydroxy-2-naphthoic acid	3279	2229	3280	2230	3280	2210+2229
27	2,5-Xylenol	3280	2229	3279	2229	3280	2230
28	Salicylic acid	3280	2230	3279	2229	3280	2210+2222+2229
29	m-Nitrobenzoic acid	3282	2215+2229	3295	2215+2230	3295	2215
30	Skatole	3278	2229	3280	2216+2230	3289	2216
31	Hydroquinone	3279	2229	3279	2210+2229	3280	2223+2230
32	Fumaric acid	3279	2229	3280	2209+2230	3279	2229
33	Methyl gallate	3280	2230	3280	2230	3281+3303	2209+2230
34	p-Cresol	3279	2229	3281	2209+2230	3279+3303	2210+2229
35	Methanesulfonic acid	3279	2229	3282+3301	2209+2230	3280	2230
36	p-Ethylphenol	3280	2210+2230	3281	2229	3280	2230
37	3-Hydroxybenzoic acid	3280	2230	3278	2229	3281	2222+2230
38	6-Hydroxy-2-naphthoic acid	3280	2230	3294	2218	3281	2222+2230
39	Ethanesulfonic acid	3280	2229	3282+3301	2210+2223	3274	2214+2226
40	Allocitric acid	3279	2230	3280	2229	3280	2222+2230
41	p-tert-butylphenol	3280	2210+2230	3279	2209+2229	3280+3303	2210+2230
42	3,4-Xylenol	3280	2230	3279	2209+2230	3280	2230
43	2,6-Xylenol	3281+3301	2209+2230	3284+3302	2209+2230	3279+3301	2209+2229
44	Citric acid	3280	2210+2230	3280	2211+2229	3278	2223+2229
45	Etidronic acid	3279	2228	3279	2229	3279	2229
46	4-Hydroxybenzoic acid	3280	2229	3281	2211+2229	3281	2219
47	o-Phenylphenol	3279	2211+2229	3279	2229	3303	2208
48	2-Oxo-3-phenylpropionic acid	3279	2229	3278	2229	3281	2215+2229

The wavenumbers listed in Table S11 are all explained by conversion of ROY polymorphs as the peak maximums observed are all commensurate (within the accuracy of the instrument used) with those obtained for one or more polymorphs of ROY.

7. DSC data for ROY and pyrogallol

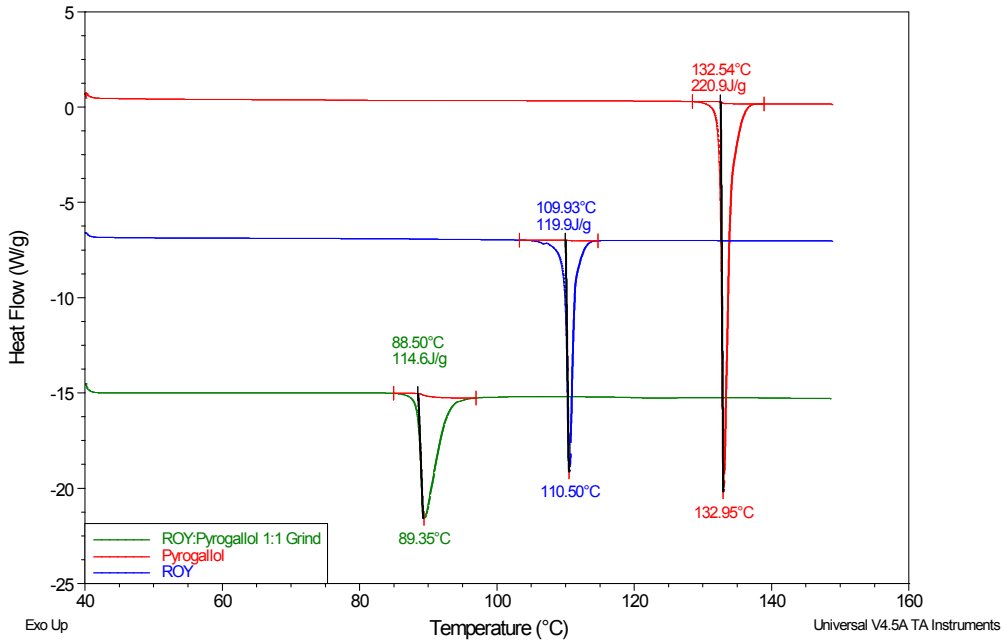

Figure S12. Initial heating phase DSC curves of Pyrogallol (red), ROY (blue) and ROY:Pyrogallol 1:1 grind (green).

In Figure S12 single melting points are seen for ROY, Pyrogallol and a single lower melting point observed for the 1:1 grind of these two components.

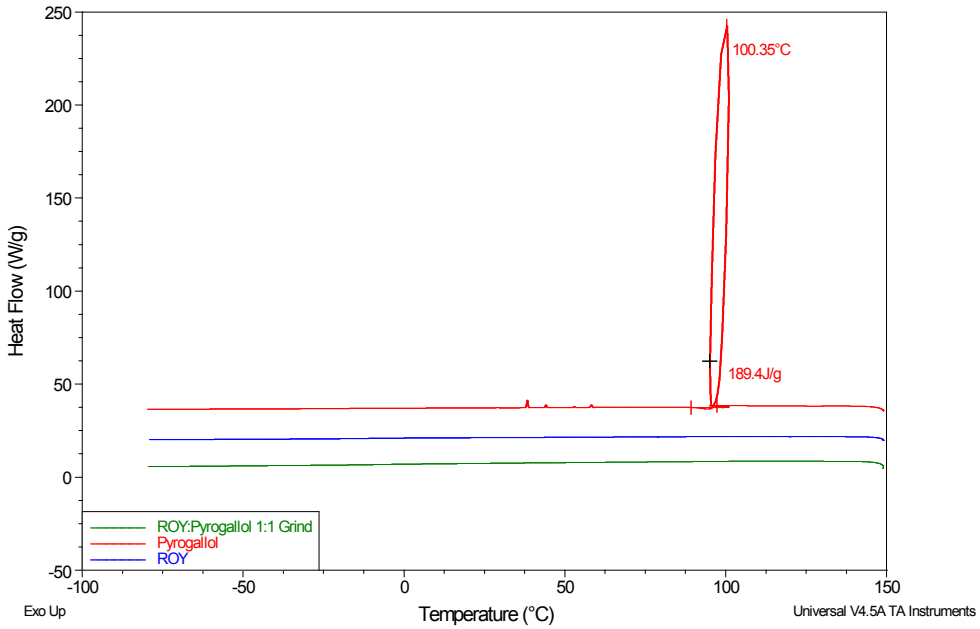

Figure S13. Cooling phase DSC curves of Pyrogallol (red), ROY (blue) and ROY:Pyrogallol 1:1 grind (green).

Figure S13 shows the exothermic peak associated with the crystallisation of pyrogallol which occurs on cooling.

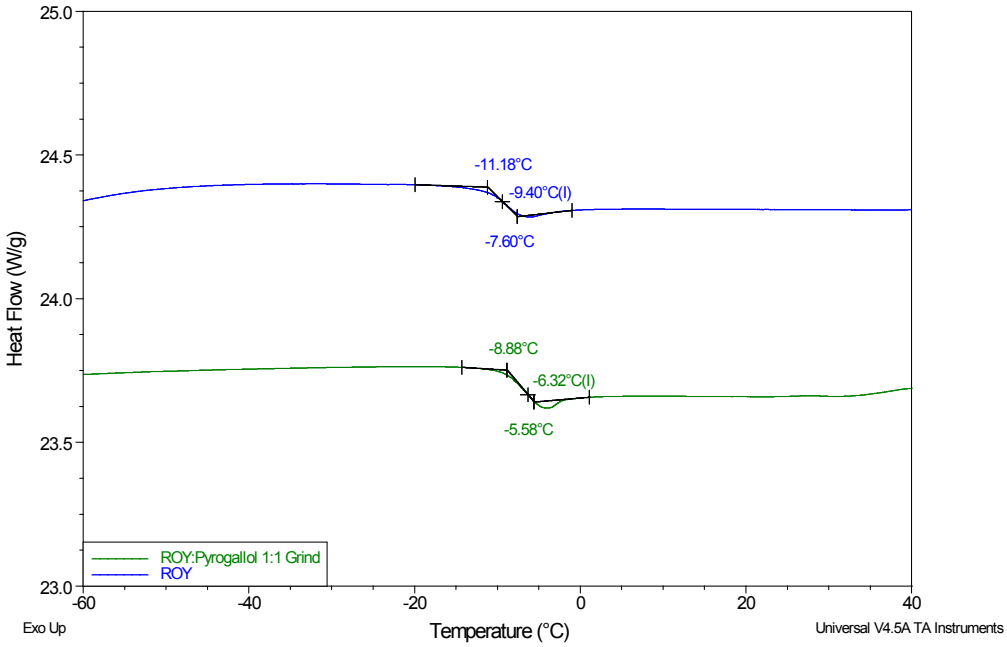

Figure S14. Focused area of second heating cycle DSC curves of ROY (blue) and ROY:Pyrogallol 1:1 grind (green) showing glass transitions.

ROY and the ROY:Pyrogallol 1:1 grind do not crystallise on cooling (Figure S13), instead forming amorphous phases with observable glass transitions (Figure S14). These occur, on heating, at around -9.4°C and -6.3°C respectively.

In order to determine whether this effect was maintained across varying stoichiometry a number of blends of ROY:pyrogallol were prepared. Figure S15 shows the initial endotherms for the ground mixtures. Displaying a consistent peak at around 88.5°C with a diminishing heat of fusion. This is indicative that the same interaction is maintained but to an extent that reduces in line with composition. The latter two peaks correlate well to the melting points of polymorphs (YT04 & OP) of ROY.[1]

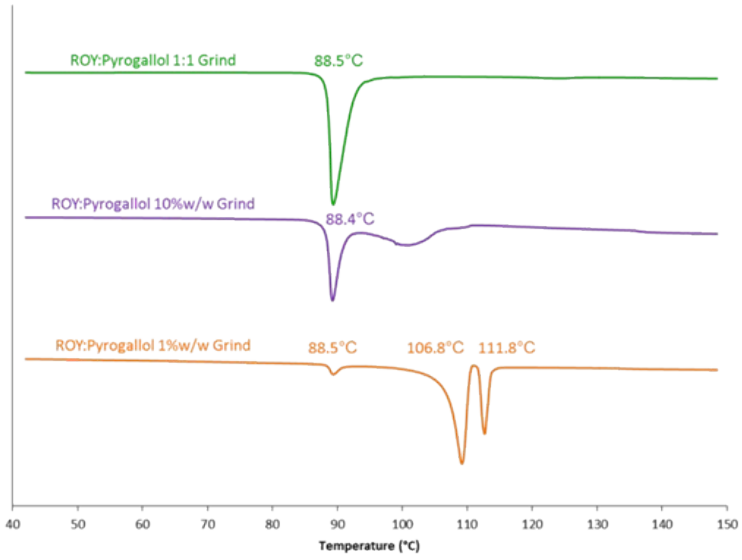

Figure S15. Initial melting points for grinds of varying ratio of ROY:Pyrogallol content.

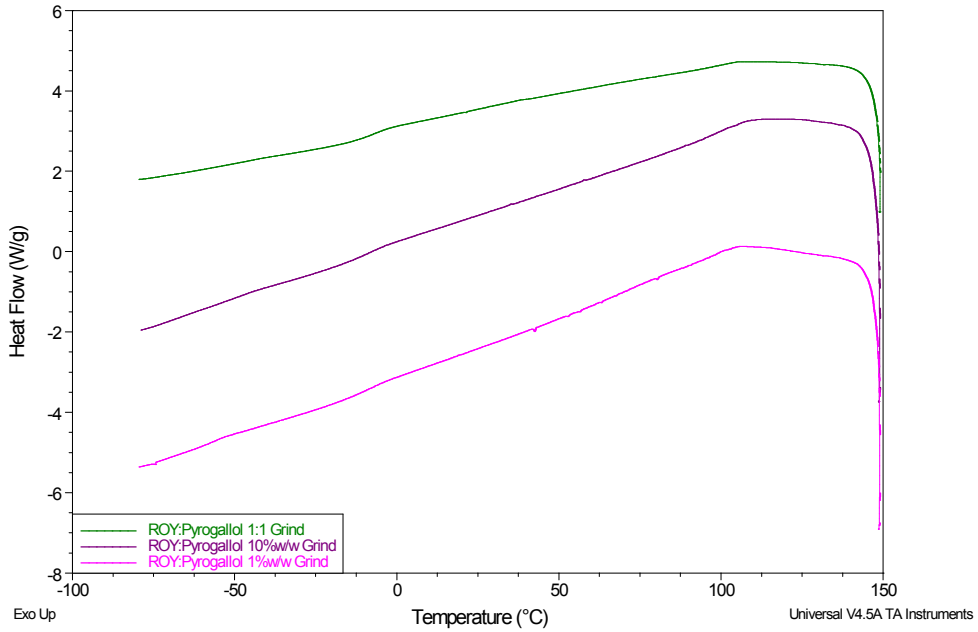

Figure S16. Cooling phase DSC curves of ROY:Pyrogallol: 1:1 grind (green), 10%w/w (purple) and 1%w/w (pink). All displaying no recrystallization and a glass transition at around -8°C.

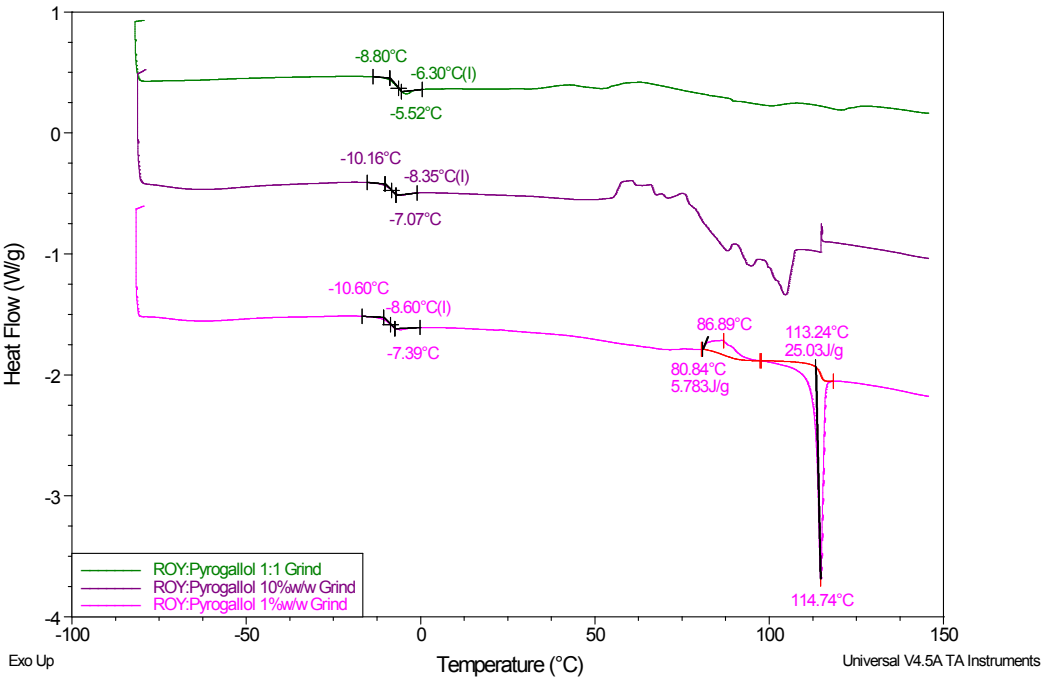

Figure S17. Second heating phase DSC curves of ROY:Pyrogallol 1:1 grind (green), 10%w/w (purple) and 1%w/w (pink) including glass transitions.

Figures S15 to S17 show that the ROY:Pyrogallol grinds containing 10%w/w and 1%w/w pyrogallol display similar behaviour to the 1:1 grind in that crystallisation does not occur during the cooling cycle and that glass transition are observed, occurring slightly lower at around -8.4°C and -8.6°C respectively. The most significant difference is observed during the second heating phase in which exothermic events occur for the two samples with lower pyrogallol content, indicative of recrystallization.

To further analyse the 1:1 nature of the interaction a range of ROY:Pyrogallol grind samples were produced from 5% to 95% pyrogallol content and analysed by DSC heating from ambient, at 10°C/min, to 150°C. The initial melting point for each of these samples, on the first heating cycle, fell within a narrow range (see Figure S18, below).

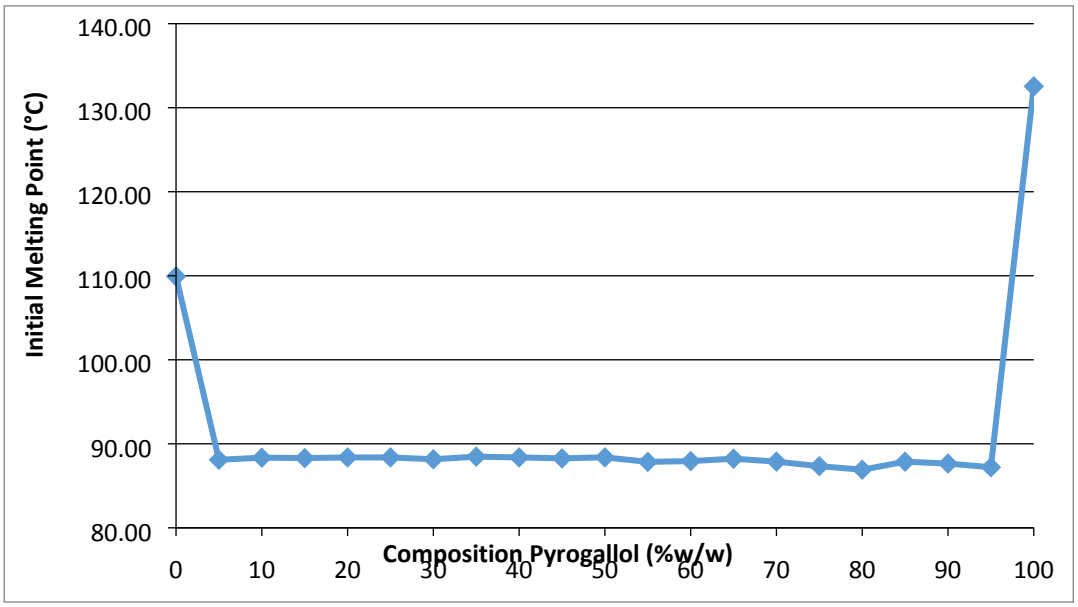

Figure S18. Initial melting points for grinds of varying ratio of ROY:Pyrogallol content. Melting points range between 86.92 to 88.47°C for 5-95%w/w pyrogallol.

8. Interaction determination

In order to explore the nature of the interactions between ROY and pyrogallol in the amorphous form hydrogen bond propensity prediction and an amorphous cell were produced.

Tables S18-21 show the parameters for and outputs from hydrogen bonding propensity calculations applied to ROY and aromatic hydroxyl groups representing pyrogallol using the logit hydrogen-bonding propensity (LHP) model.[2]

This predicted no strong hydrogen bond potential between ROY and pyrogallol. Predicting only self-self interactions in ROY.

Table S19. Coefficients for logit_model_1 applied to ROY (QAXMEH01).

Coefficients:	Estimate	Std.Error	Z value	Pr(>|z|)	Significance code	Lower Bound	Upper Bound
(Intercept)	**0.633**	0.234	2.709	0.00675519	**	0.165	1.083
Donoratom_2_of_ar_hydroxy	**-0.391**	0.074	-5.258	1.45444e-07	***	-0.537	-0.246
Donorother	**0.611**	0.066	9.221	2.9478e-20	***	0.482	0.742
Acceptoratom_2(3)_of_ar_nitro	**2.242**	0.195	11.519	1.06424e-30	***	1.874	2.639
Acceptoratom_2_of_ar_hydroxy	**1.883**	0.193	9.756	1.73657e-22	***	1.519	2.277
Acceptoratom_2_of_cyano	**2.361**	0.196	12.017	2.89222e-33	***	1.989	2.761
Acceptorother	**4.313**	0.183	23.549	1.28037e-122	***	3.969	4.689
competition	**-0.086**	0.005	-17.931	6.78803e-72	***	-0.096	-0.077
Donor_steric_density	**-0.023**	0.002	-12.486	8.87143e-36	***	-0.027	-0.019
Acceptor_steric_density	**-0.045**	0.002	-20.515	1.58124e-93	***	-0.050	-0.041
Donor_aromaticity	**-0.805**	0.177	-4.545	5.49985e-06	***	-1.154	-0.459
Acceptor_aromaticity	**-0.529**	0.164	-3.228	0.00124467	**	-0.850	-0.208
Donoratom_0_of_sec_amine_1	**0.000**	N/A	N/A	N/A	N/A	N/A	N/A
Acceptoratom_1_of_cyclic_thioether	**0.000**	N/A	N/A	N/A	N/A	N/A	N/A

Table S20. Goodness of fit.

Log Likelihood	-5207.380
Area under ROC curve	0.860968
Akaike Information Criterion (AIC)	10438.8
Null deviance	15325.3 on 11218 degrees of freedom
Residual deviance	10414.8 on 11207 degrees of freedom

Table S21. Predicted inter-molecular hydrogen bond propensities.

Donor	Acceptor	competition	Donor steric density	Acceptor steric density	Donor aromaticity	Acceptor aromaticity	**Propensity**	Lower bound	Upper bound	Frequency
N1 of sec_amine_1	N3 of cyano	4.00	62.75	27.57	0.58	0.58	**0.31**	0.22	0.42	36.8
N1 of sec_amine_1	O2 of ar_nitro	4.00	62.75	31.19	0.58	0.58	**0.25**	0.17	0.35	11.7
N1 of sec_amine_1	O1 of ar_nitro	8.00	62.75	31.19	0.58	0.58	**0.19**	0.13	0.28	18.2
N1 of sec_amine_1	S1 of cyclic_thioether	8.00	62.75	62.75	0.58	0.58	**0.01**	0.01	0.01	1.1

Table S22. Predicted intra-molecular H-bond propensities.

Donor	Acceptor	Donor sybyl atom type	DA Pair constrained connectivity	DA Pair path string	Donor count	**Propensity**	Lower bound	Upper bound
N1	O1	N.pl3	1	0	1	**0.890416**	0.890416	0.890416
N1	O2	N.pl3	1	0	1	**0.890416**	0.890416	0.890416
N1	N3	N.pl3	1	0	1	**0.0918711**	0.0918711	0.0918711

An amorphous cell constructed with 200 molecules (100 ROY, 100 pyrogallol) showed similar strong H-bond behaviour (S23-25) to that which was predicted by the propensity tool correlated to that seen in IR experimentation.

N.B. strong H-bonds were defined by a X-H distance of 3Å and analysed in Mercury (CCDC).

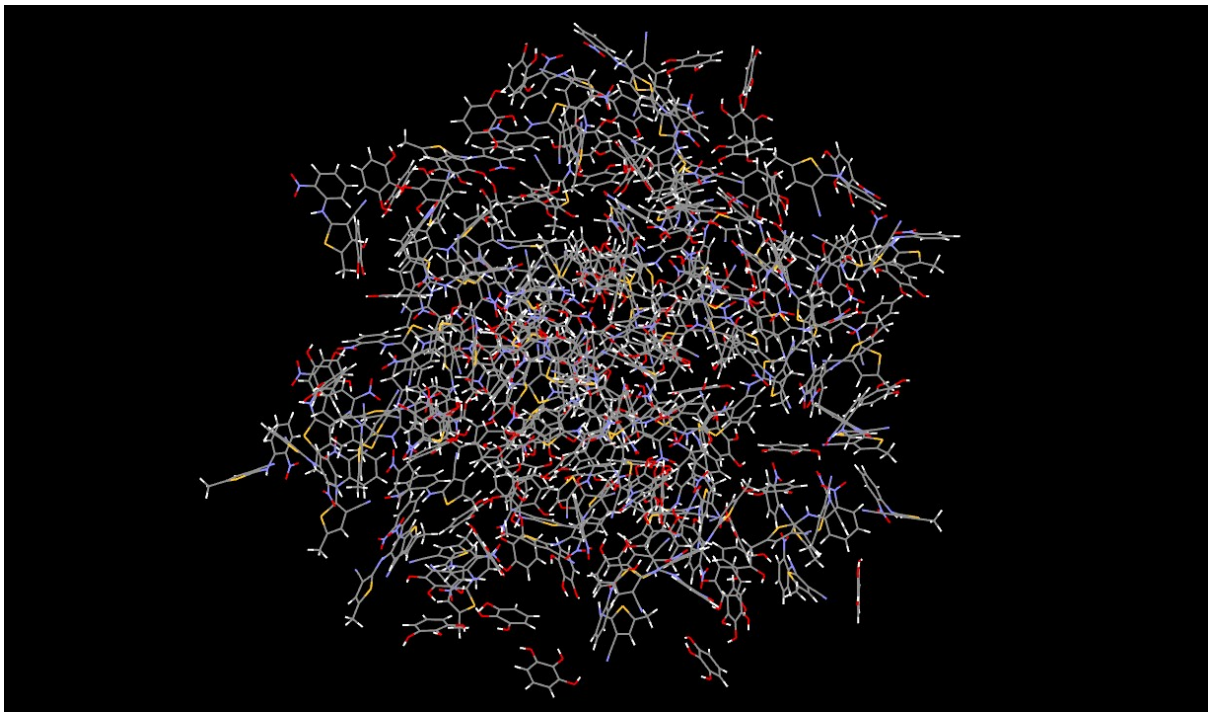

Figure S23. Amorphous cell displaying all 200 molecules. 100 pyrogallol and 100 ROY.

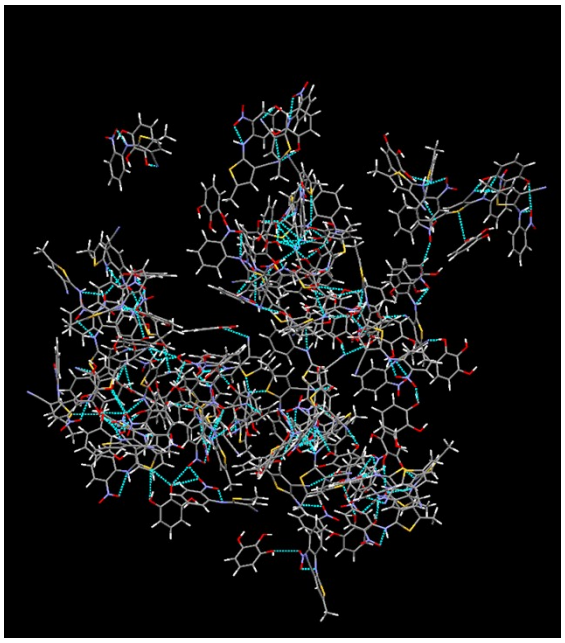

Figure S24. Amorphous cell displaying strong H-bond contacts between ROY and pyrogallol. N.B. All non-bonded molecules and those containing ROY:ROY contacts and pyrogallol:pyrogallol have been removed to enable some degree of clarity. The minimised cell is available as an additional ESI file.

These interactions were further analysed with the output displayed in Table S25.

Table S25. Number of strong H-bond contacts in the amorphous cell between molecules.
*The interactions between ROY and pyrogallol were supported by a total of 44 pyrogallol molecules. i.e. Some molecules supported more than one interaction. A further 32 pyrogallol molecules bonding self:self and 24 taking no part in any strong H-bonding.

Molecule (group) 1	**Molecule (group) 2**	**Number**
ROY (nitro)	ROY (amine)	100 (all) intramolecular bond
Pyrogallol (OH)	Pyrogallol (OH)	32
ROY (nitro)	Pyrogallol (OH)*	20
ROY (cyano)	Pyrogallol (OH)*	32
ROY (amine)	Pyrogallol (OH)*	4
ROY (sulfur)	Pyrogallol (OH)*	8

These results correlate with the H-bond propensity prediction and IR data, as all ROY molecules possess the characteristic intra-molecular bond (propensity) and pyrogallol would be expected to alter the environment of this through its interaction (IR).

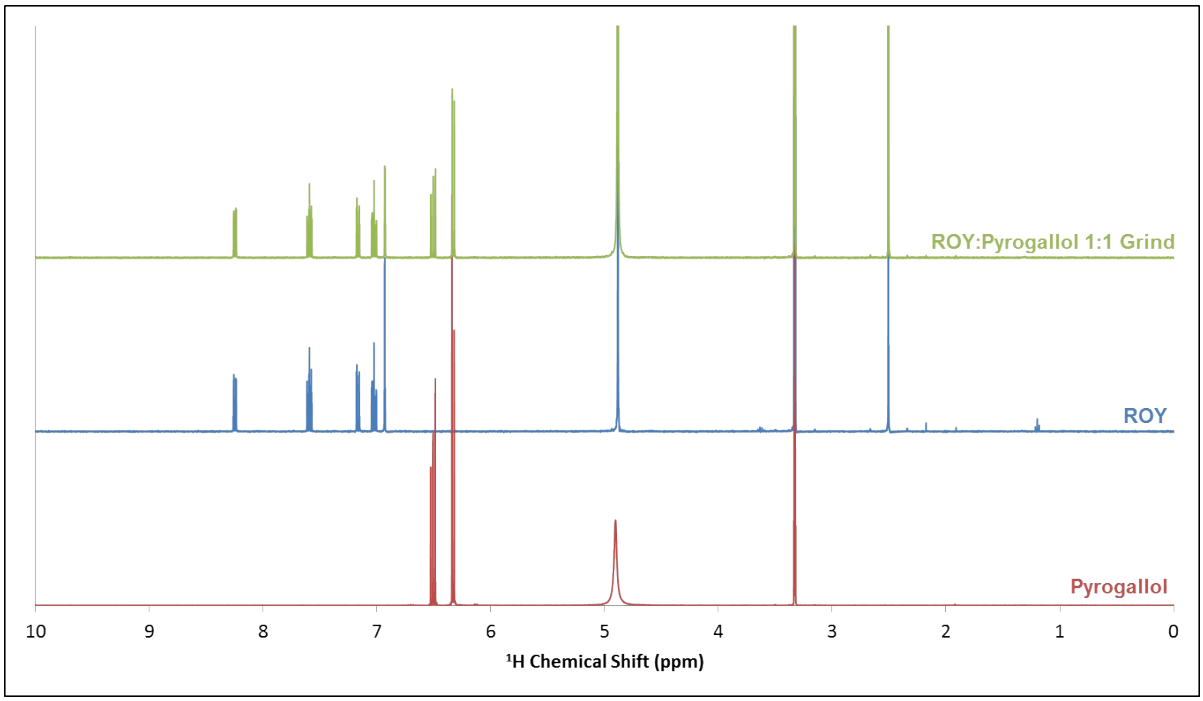

Figure S26. ^{1}H NMR spectra of ROY (blue), Pyrogallol (red) and the grind, integrates to a 1:1 molar ratio of the two (green).

9. DSC data for ROY and PVP

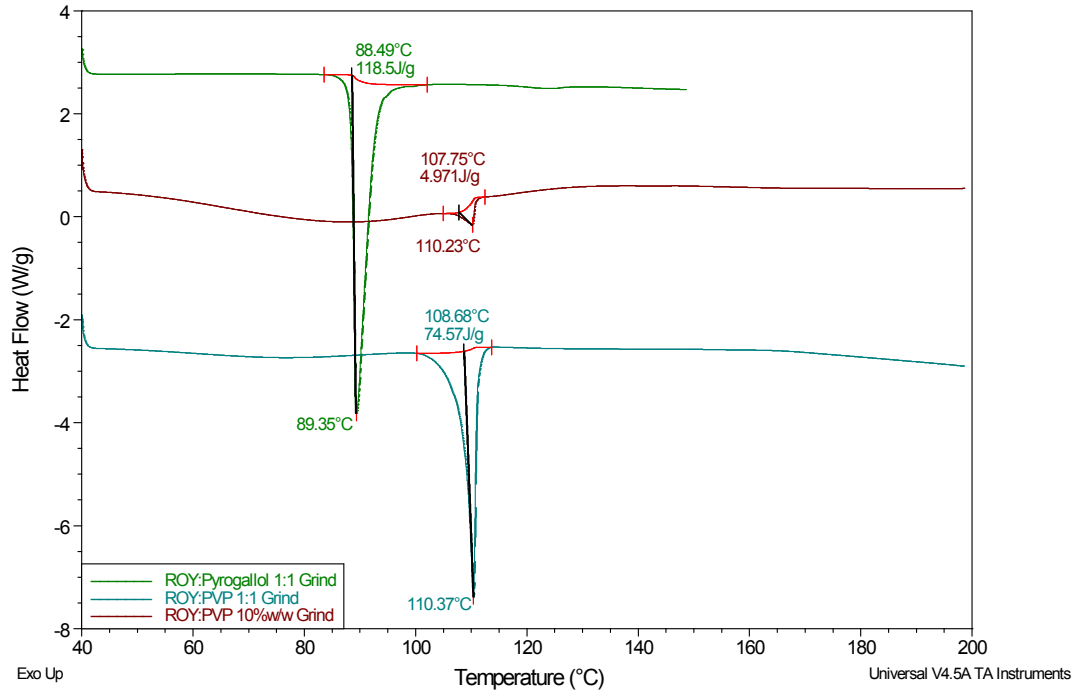

Figure S27. Initial heating phase DSC curves of ROY:Pyrogallol 1:1 grind (green), ROY:PVP 1:1 grind (teal) and ROY:PVP 10%w/w grind (maroon).

The melting points observed in the ROY:PVP samples (Figure S27) do not display the same reduction in melting point seen with the ROY:Pyrogallol samples and instead display melting points within the range of those of pure ROY. The ROY:PVP 1:1 grind having a larger endotherm compared to the sample with 10%w/w ROY corresponding to the greater quantity of ROY present.

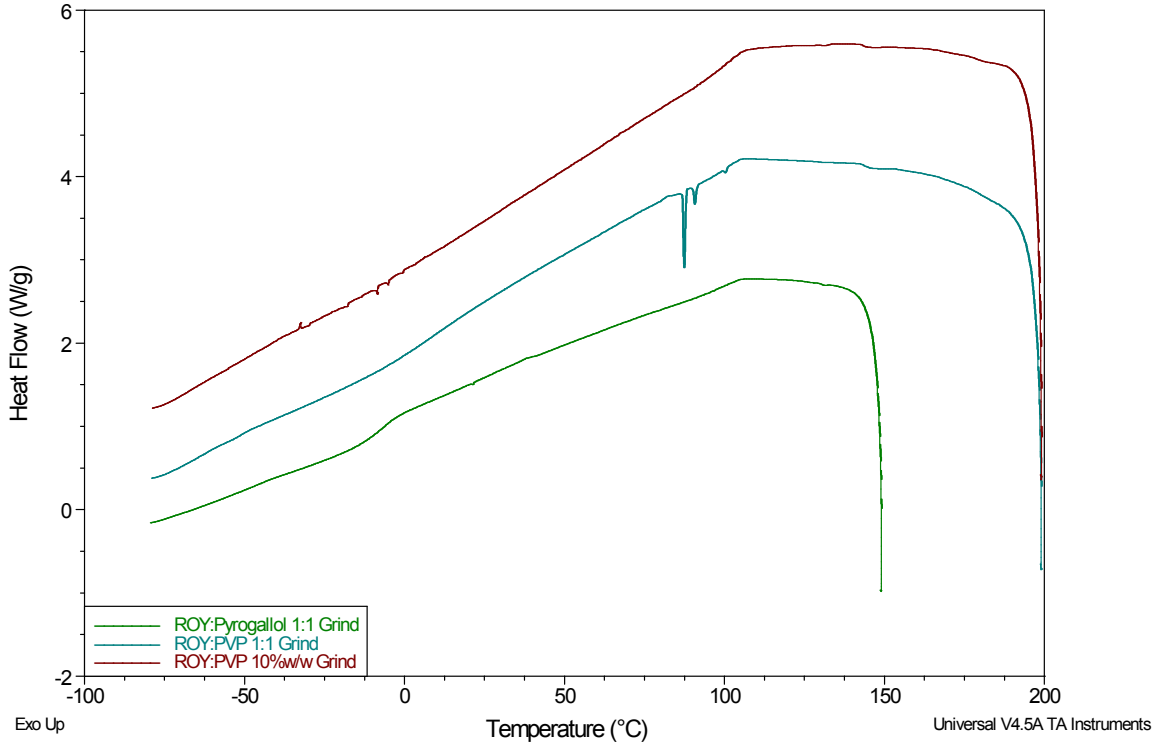

Figure S28. Cooling phase DSC curves of ROY:Pyrogallol 1:1 grind (green), ROY:PVP 1:1 grind (teal) and ROY:PVP 10%w/w grind (maroon).

The behaviour of the materials during the cooling and second heating cycles correspond well with those of the ROY:Pyrogallol 1:1 grind given that crystallisation is not evident in either cycle indicated by the lack of exotherms in either Figure S28 or S29.

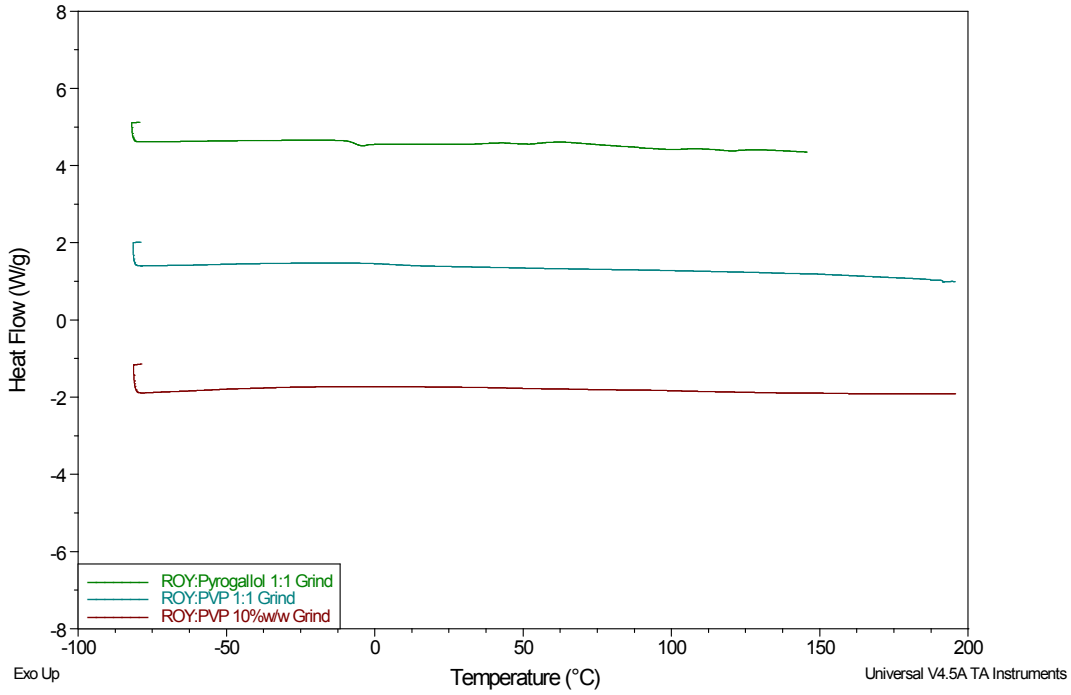

Figure S29. Second heating phase DSC curves of ROY:Pyrogallol 1:1 grind (green), ROY:PVP 1:1 grind (teal) and ROY:PVP 10%w/w grind (maroon).

10. PXRD data

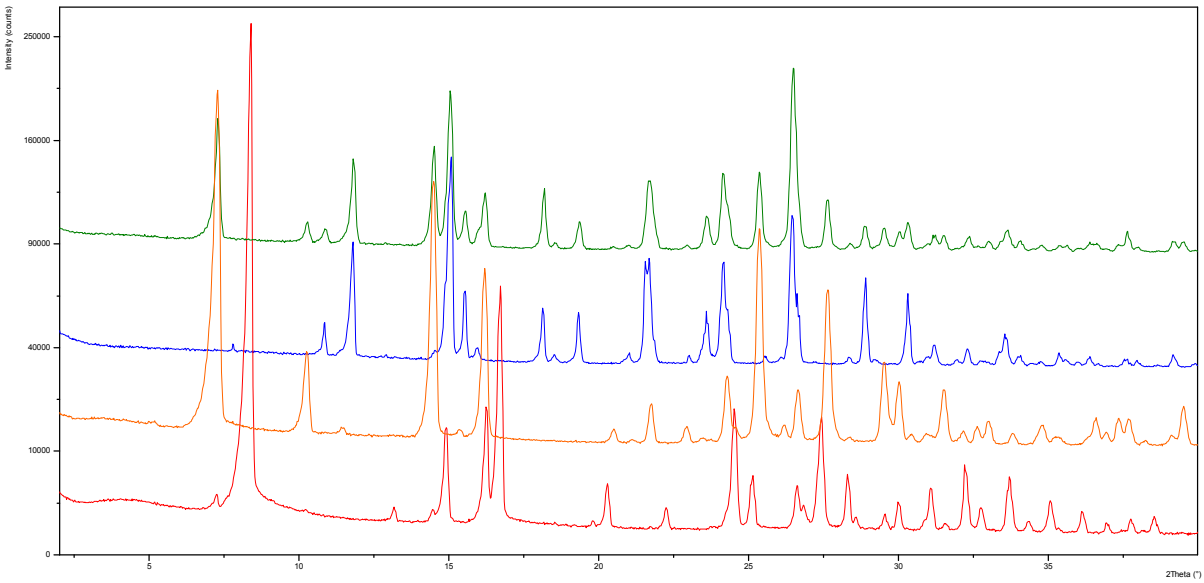

Figure S30. XRPD patterns of ROY (polymorph Y) (blue), ROY:Pyrogallol 1:1 grind (green), Pyrogallol (red) and Pyrogallol post-DVS (orange).

It is evident from the PXRD data that there is no new form seen in the product of the ROY:pyrogallol grinding experiment. A new but explicable peak is observed in the sample. This peak at around 14.5° 2θ can also be seen in the post-DVS pyrogallol sample which had hydrated to the pyrogallol tetarto-hydrate and this gives rise to the peaks in Figure S30. The DVS plots for pyrogallol can be seen in Figure S31 below.

11. Dynamic Vapour Sorption (DVS) analysis of pyrogallol and PVP

DVS was undertaken using an Surface Measurement Systems (London UK) DVS-1 with a 10% RH step between humidity values with equilibrium achieved at 0.1% weight change before moving to the next step. Methods were started at the humidity of the room at ambient (measured by a Rotronic A/H hygrometer) with subsequent increase to 90%RH before cycling to 0%RH, to 90%RH, to 0%RH. Sample weights of between 5-20mg were used for all samples.

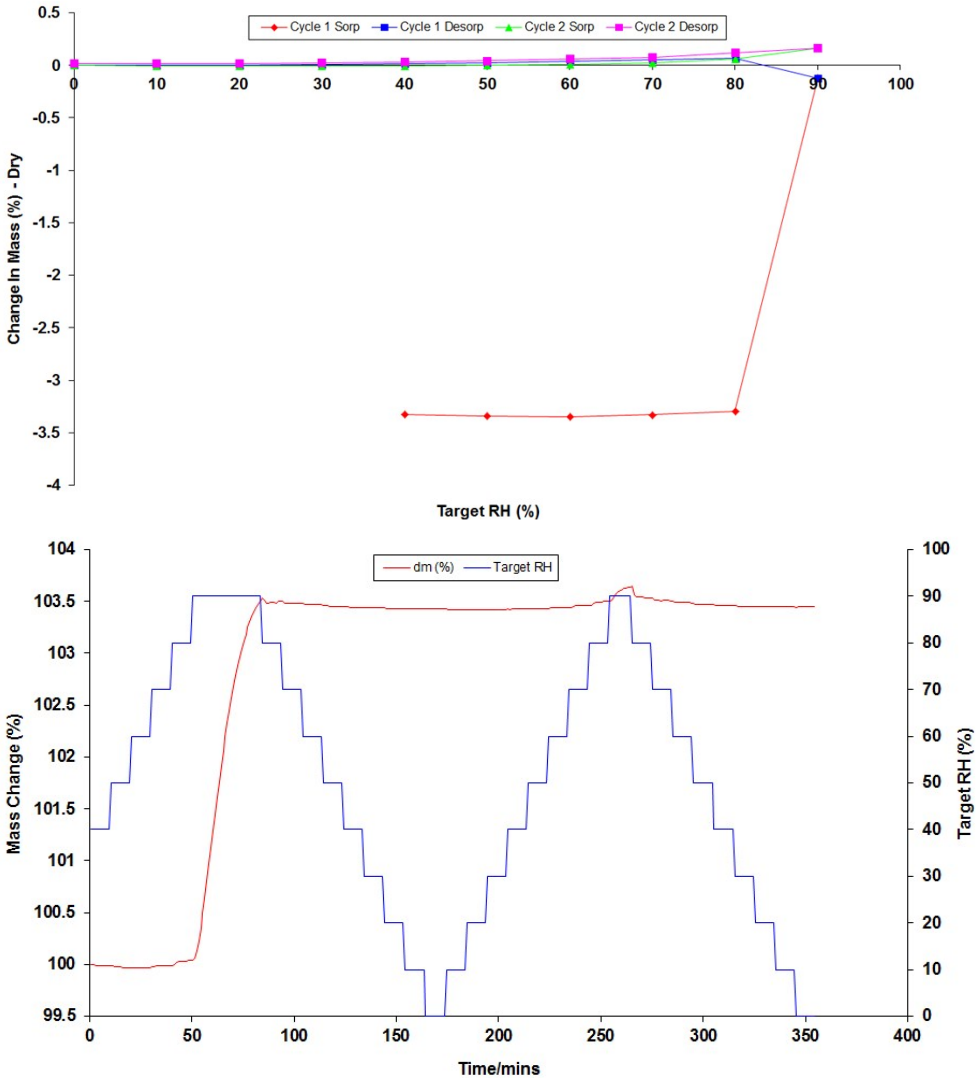

Figure S31. Isotherms (top) and change in mass plot (bottom) for pyrogallol. N.B. see scale.

In the initial sorption cycle relative humidity above 80% displays moisture uptake indicative of an absorption of ¼ mole of water seen in Figure S26, this is followed by very little change against humidity in the following desorption/sorption cycles. This indicates that the pyrogallol sample hydrated from its initial form. In this case there is approximately 3.3% change in mass correlating to the tetarto-hydrate being formed. [3,4]

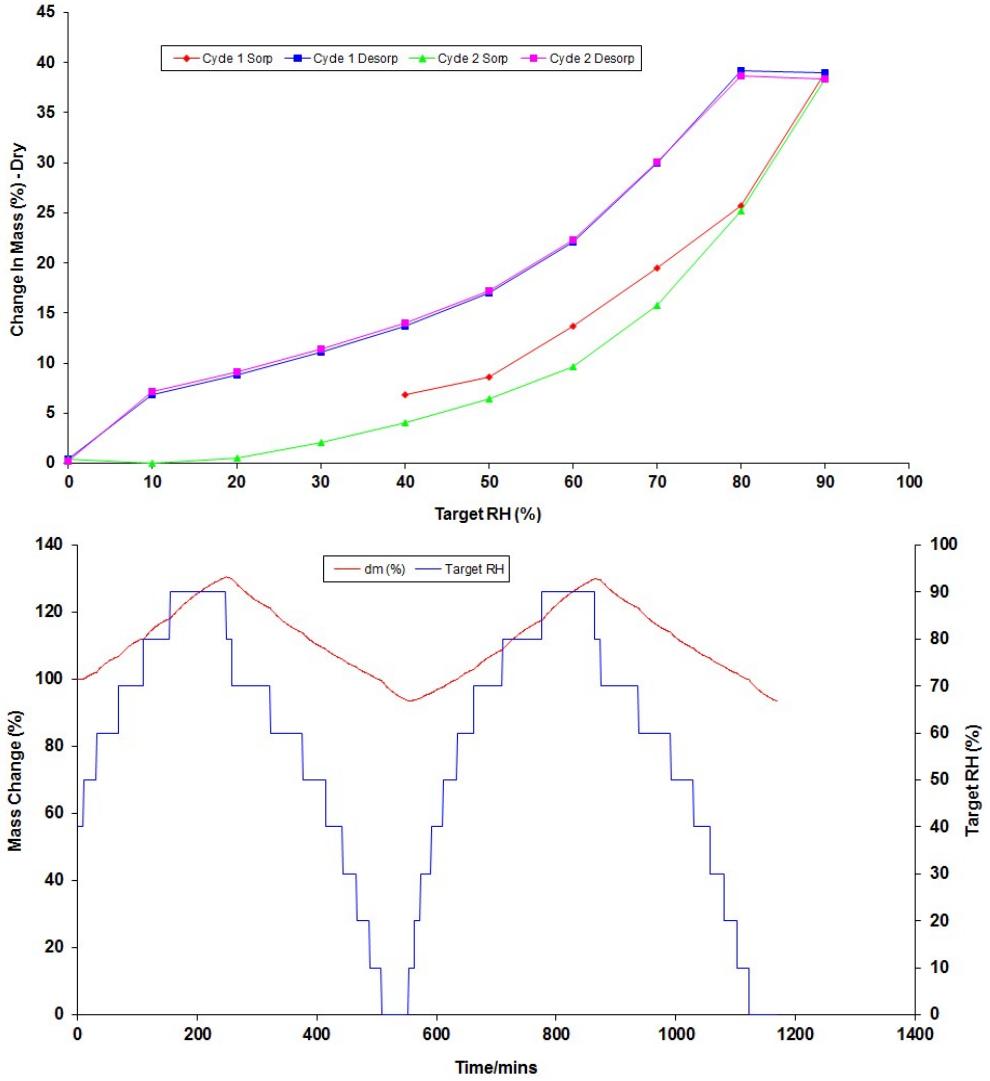

Figure S32. Isotherms (top) and change in mass plot (bottom) for PVP. N.B. see scale.

PVP displays much greater hygroscopicity across the humidity range tested (Figure S32) than that of pyrogallol. Use of a material which displays greater resistance to moisture uptake, such as pyrogallol, especially at lower humidity levels, may prove beneficial for use as an amorphous stabilising agent where the uptake of water can negatively impact the stability of the phase.

12. Stability of the ROY:Pyrogallol co-amorphous material

Investigation of the stability of the co-amorphous material included determination of the phase's stability to moisture. No DVS data could be collected on the phase due to recrystallization in the instrument. Further stability analysis was conducted by DSC and PXRD.

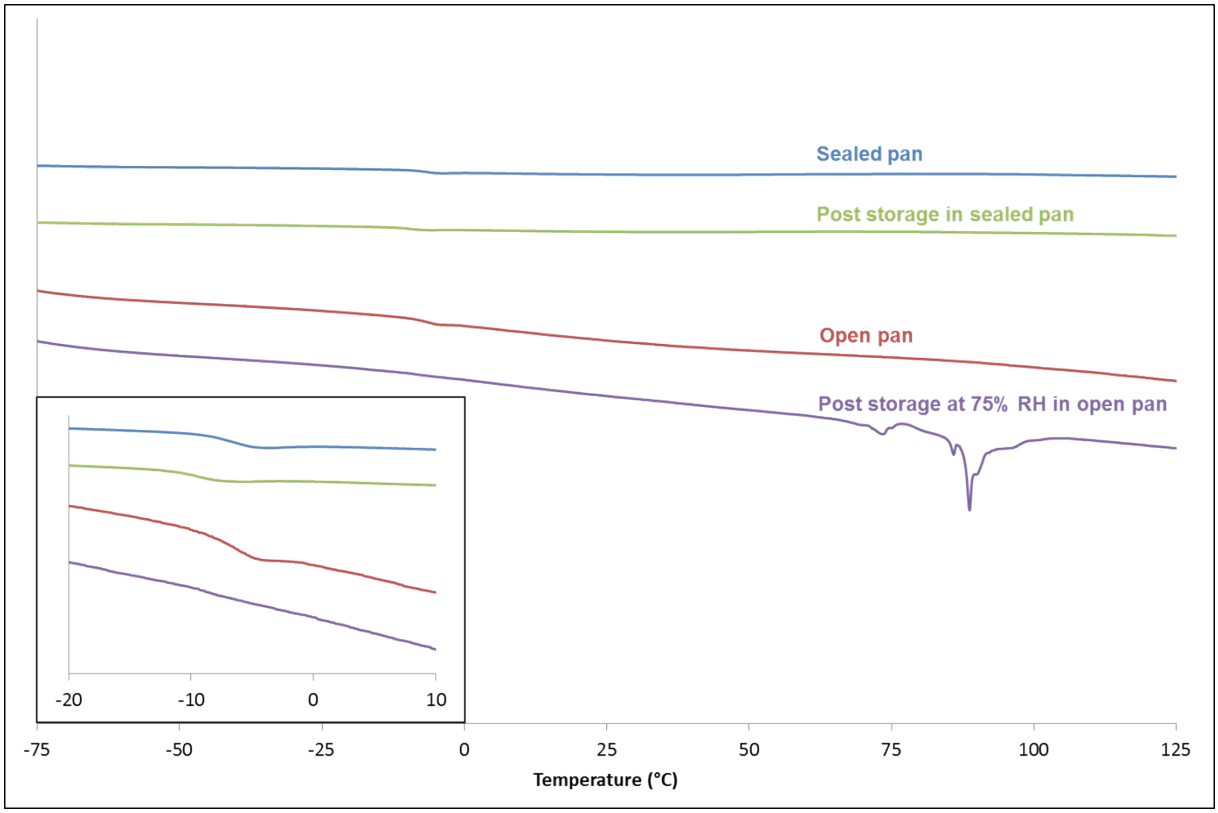

Figure S33. Heating phase DSC curves of ROY:Pyrogallol 1:1 grind: in sealed DSC pan (blue), after storage in sealed DSC pan for approximately 65 hours (green), in an open DSC pan (red) and after storage at 75% RH in an open DSC pan (purple). Presence of Tg in all samples except that stored at 75% RH (purple) are highlighted in the inset.

The blue DSC trace is of the initial ground sample of 1:1 ROY:Pyrogallol, which was sealed within a standard DSC pan and subjected to the same heat-cool-heat method as previous samples. This sample was left sealed at RT for approximately 65 hours and then a cool-heat method (cool at 10°C/min from 25°C to -90°C then heat at 10°C/min to 150°C) which gave the green DSC trace. As is evident, no crystallisation has occurred and the sample remains in the amorphous state. Another ground sample of 1:1 ROY:Pyrogallol was placed in an open Tzero aluminium DSC pan (no lid added) and the heat-cool-heat method run giving rise to the red trace. This sample was placed in a 75% relative humidity environment and was visually seen to crystallise immediately, with the purple trace generated around 18 hours later (cool-heat method) resulting in the purple trace. This evidence suggests that crystallisation from the amorphous phase is mediated by an increased humidity.

Samples were also prepared of ROY and the 1:1 co-amorphous mixture and stored at ambient conditions and monitored for crystallinity by PXRD Figure S34 and S35.

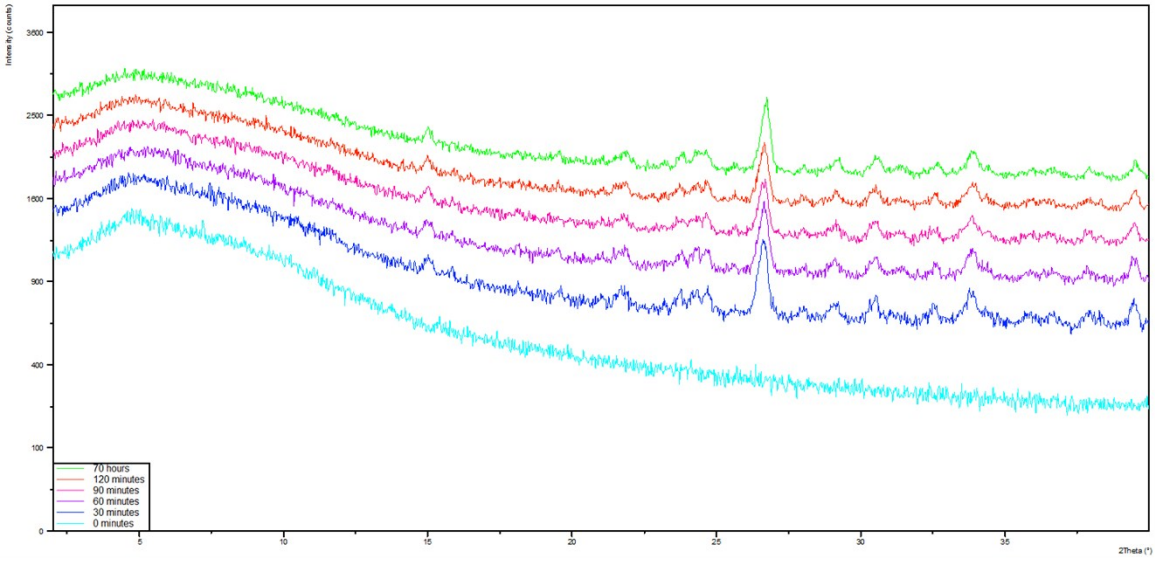

Figure S34. Evolution of crystallinity over a 70 hour period from an amorphous droplet of pure ROY, scan lengths of approximately 10 minutes at 30 minute intervals for 2 hours and a final scan after 70 hours.

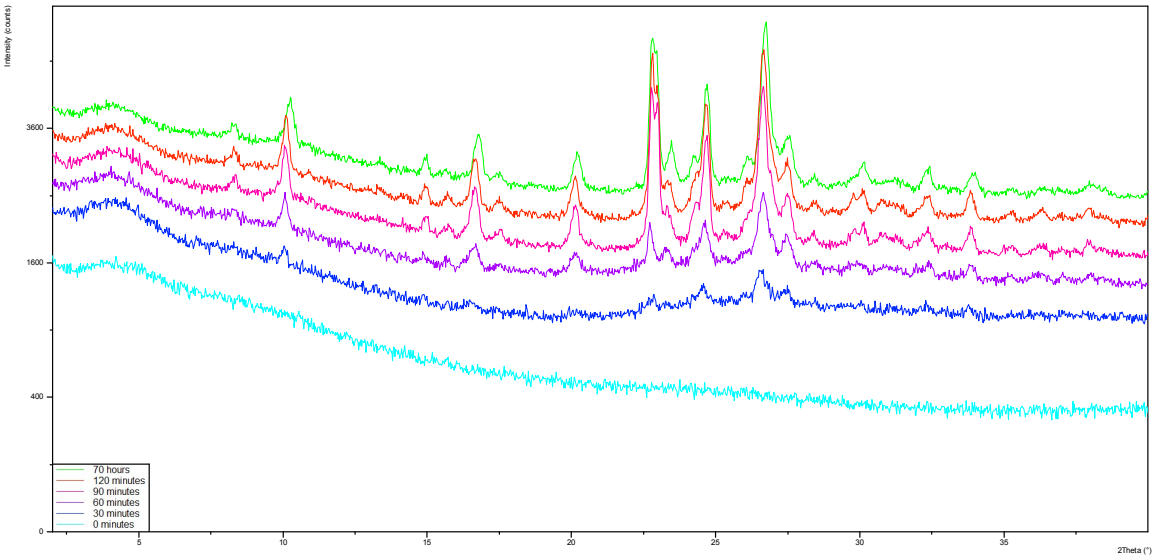

Figure S35. Evolution of crystallinity over a 70 hour period from an amorphous droplet of ROY:Pyrogallol 1:1 Grind, scan lengths of approximately 10 minutes at 30 minute intervals for 2 hours and a final scan after 70 hours. These data show recrystallization of both ROY and pyrogallol as per Figure S30.

In this case, crystallisation appears to have occurred earlier in the ROY sample than the co-amorphous mixture. In this sample crystallinity is seen at 15 minutes with no change in crystallinity at 70 hours, as seen by the lack of change in patterns between these times. In contrast the ROY:Pyrogallol data suggests a gradual increase in crystallinity from the 15-minute scan to at least 90 minutes.

References

1. L. Yu, *Acc. Chem. Res.*, 2010, **43**, 1257–66.

2. P. T. A. Galek, L. Fábián, W. D. S. Motherwell, F. H. Allen, and N. Feeder, *Acta Crystallogr. Sect. B Struct. Sci.*, 2007, **63**, 768–782.

3. R. Thakuria, S. Cherukuvada, and A. Nangia, *Cryst. Growth Des.*, 2012, **12**, 3944–3953.

4. D. E. Braun, R. M. Bhardwaj, J. B. Arlin, A. J. Florence, V. Kahlenberg, U. J. Griesser, D. A. Tocher, and S. L. Price, *Cryst. Growth Des.*, 2013, **13**, 4071–4083.